

UINO-FSS: Unifying Representation Learning and Few-shot Segmentation via Hierarchical Distillation and Mamba-HyperCorrelation

Wei Zhuo, Zhiyue Tang, Wufeng Xue[†], *Member, IEEE*, Hao Ding, Junkai Ji, Linlin Shen[†], *Senior Member, IEEE*

Abstract—Few-shot semantic segmentation has attracted growing interest for its ability to generalize to novel object categories using only a few annotated samples. To address data scarcity, recent methods incorporate multiple foundation models to improve feature transferability and segmentation performance. However, they often rely on dual-branch architectures that combine pre-trained encoders to leverage complementary strengths, a design that limits flexibility and efficiency. This raises a fundamental question: “*can we build a unified model that integrates knowledge from different foundation architectures?*” Achieving this is, however, challenging due to the misalignment between class-agnostic segmentation capabilities and fine-grained discriminative representations. To this end, we present UINO-FSS (pronounced /juːˈɑːnəʊ/), a novel framework built on the key observation that early-stage DINOv2 features exhibit distribution consistency with SAM’s output embeddings. This consistency enables the integration of both models’ knowledge into a single-encoder architecture via coarse-to-fine multimodal distillation. In particular, our segmenter consists of three core components: a bottleneck adapter for embedding alignment, a meta-visual prompt generator that leverages dense similarity volumes and semantic embeddings, and a mask decoder. Using hierarchical cross-model distillation, we effectively transfer SAM’s knowledge into the segmenter, further enhanced by Mamba-based 4D correlation mining on support-query pairs. Extensive experiments on PASCAL-5ⁱ and COCO-20ⁱ show that UINO-FSS achieves new state-of-the-art results under the 1-shot setting, with mIoU of 80.6 (+3.8%) on PASCAL-5ⁱ and 64.5 (+4.1%) on COCO-20ⁱ, demonstrating the effectiveness of our unified approach.

Index Terms—Few-shot semantic segmentation, knowledge distillation, visual prompt generation.

I. INTRODUCTION

SEMANTIC segmentation, which performs pixel-wise classification, has achieved great success in recent years. However, these methods usually require extensive training on large-scale, densely annotated datasets. To mitigate the burden

[†] Wufeng Xue and Linlin Shen are the corresponding authors.

Wei Zhuo, Zhiyue Tang, Hao Ding, and Junkai Ji are with the School of Artificial Intelligence and the National Engineering Laboratory of Big Data System Computing Technology, Shenzhen University, Shenzhen 518060, China. Wei Zhuo is also with the Guangdong Provincial Key Laboratory of Intelligent Information Processing, China (e-mail: weizhuo@szu.edu.cn, tangzhiyue2023@email.szu.edu.cn, 2400671002@mails.szu.edu.cn, jijunkai@szu.edu.cn).

Wufeng Xue is with School of Biomedical Engineering, Shenzhen University Medical School, Shenzhen University, Shenzhen 518060, China (e-mail: xuewf@szu.edu.cn).

Linlin Shen is with the School of Artificial Intelligence and the National Engineering Laboratory of Big Data System Computing Technology, Shenzhen University, Shenzhen 518060, China, and also with the Department of Computer Science, University of Nottingham Ningbo China, Ningbo 315100, China (e-mail: llshen@szu.edu.cn).

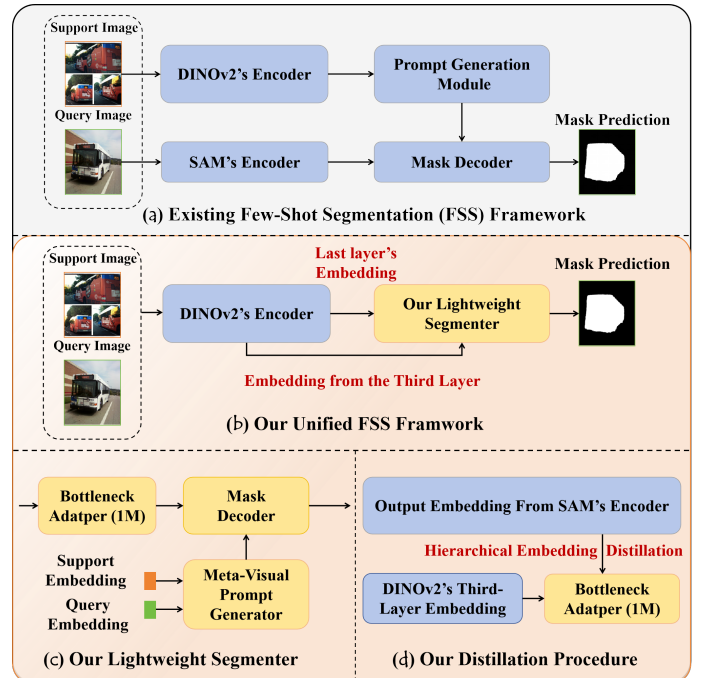


Fig. 1. **Introduction of our framework.** Our framework (b) is unified and efficient compared to the existing dual-modal architectures [1]–[3] shown in (a). Our lightweight segmenter (c) only contains 5.6M parameters, but gains knowledge from the powerful SAM via the procedure in (d).

of manual annotation, Few-shot Semantic Segmentation (FSS) has attracted increasing attention. Unlike traditional semantic segmentation, FSS aims to build a generalizable framework that can segment novel classes using only a few labeled examples.

Inspired by [4], early works [5], [6] employ meta-learning to learn generalized matching models through extensive meta-tasks constructed from support-query pairs. Such a design, which closely mimics the few-shot inference, enables the learned model to be directly applied to segment novel classes without finetuning during inference. To enable effective support-query matching, prototype-based methods [7]–[12] simply match the class prototype vector with each query pixel, while approaches based on embedding aggregation [13]–[17] extensively fuse the support and query feature maps for subsequent segmentation. Here, for embedding aggregation, convolutional hypercorrelation [16] and diverse attention-based matching [13]–[15], [18] are applied. Despite these efforts, FSS still suffers heavily from the inherent limitation

of data scarcity and faces challenges in achieving stable and distinguished embeddings of novel classes.

In recent years, foundation-model-based FSS methods [19]–[22] have pushed few-shot segmentation further to new SOTA accuracy by exploiting visual representations learned from large-scale data. Among them, the DINO family [19], [20] stands out for preserving fine-grained spatial correlations, a property that makes the features almost tailor-made for dense matching in FSS. DINOv2, however, is trained with pure self-supervision without a segmentation head; its frozen backbone alone is insufficient for producing robust masks. SAM [22], on the other hand, couples a ViT image encoder with a lightweight, class-agnostic mask decoder trained on 1B+ annotated pixels, which has inspired a branch of SAM-augmented FSS pipelines [1], [2], [23], [24]. However, SAM itself also bears limitations in extracting fine-grained embeddings for categorization. To leverage the advantages of both foundation models, recent methods confront the intrinsic misalignment between SAM’s task-specific embeddings and DINOv2’s generic features, thereby resorting to a dual-branch design [1]–[3], i.e., one for local feature extraction and prompt generation, and the other for SAM-based segmentation.

Particularly, existing FSS methods based on foundation models face the following challenges: 1) Hybrid frameworks that run two separate parallel branches would inevitable lead to high computational and memory costs, resulting in low efficiency and limited development in resource-constrained scenarios; 2) Beyond computation, SAM-based FSS methods still primarily rely on geometric prompts (e.g. points or boxes), especially in training-free solutions [1], [2], [24]. These methods could be sensitive to the point prompt selection. To overcome these issues, existing methods designs bi-directional prompt selection [1] or the graph-based segment filtering and merging processes [2], which, however, also introduce more hyper-parameters; 3) ViT self-attention lets each patch aggregate global context, yet co-occurring objects in the support image would also contaminate the support features due to the *embedding coupling*, where embeddings of one object incorporate semantics from other co-occurring objects.

To this end, we propose UINO-FSS (pronounced /ju:'aməʊ/), a novel, efficient framework that *Unifies DINOv2-based representation learning and Few-Shot Segmentation*. In contrast to the heavy dual-branch architectures, we build UINO-FSS solely from the frozen DINOv2 encoder and a new lightweight segmenter. Through structural design (Fig.1(b-c)) and the hierarchical distillation (Fig.1(d)), the segmenter consolidates knowledge from both SAM and DINOv2, with reduced foreground-background embedding coupling and hyperparameter-free meta-visual prompts.

Specifically, the UINO-FSS is inspired by our pivotal findings that DINOv2’s early-stage embeddings largely resemble the SAM’s image features, suggesting the feasibility of a unified framework. To this end, upon the frozen DINOv2 encoder, we introduce a new lightweight segmenter including three key modules: the Bottleneck Adapter (BA) for feature recalibration, a Meta-Visual Prompt Generator (MVPG), and a mask decoder. In particular, the BA uses only 1M parameters to align DINOv2’s early-stage embeddings with SAM’s image

features, enabling a compact design of the segmenter. The MVPG then maintains a clean prompting process, eliminating the need for geometric prompts and handcrafted processes, by generating both semantic-aware visual prompts and correlation-based dense prompts from class prototypes and support-query correlations, respectively. The image embedding and prompts are finally imported to a mask decoder, which is initialized from SAM. For effective training, a hybrid learning strategy, combining coarse-to-fine knowledge distillation and meta-learning, is proposed for FSS. Compared to DINOv2-based FSS method [25], our knowledge consolidation leads to dramatically better performance with fewer parameters. Notably, the compact UINO-FSS, using a vanilla MVPG based on only 2D cosine similarity, can already establish a new, unified and powerful pipeline for FSS.

To further boost segmentation quality, we enhance the MVPG with a novel Mamba-based dense prompt generator, enabling foreground-background contrastive enhancement and Mamba-based hypercorrelation processing. Comparing patches between the query and support foreground, it leads to a 4D correlation volume, named hypercorrelation. Beyond [16] that decouples the hypercorrelation into 2D slices along the support and query dimensions, we introduce an efficient Mamba-Hypercorrelation Module (MHM) that processes the full volumetric similarities as an integrated 4D structure, enabling true high-order correlation modeling and fine-grained matching. The 4D correlation volume is hierarchically encoded via stacked Hierarchical Global Modeling Blocks (HGMB), which alternate between convolutions and Visual State Space (VSS) layers to progressively capture both local and global dependencies, thereby improving robustness to noise and matching accuracy. Additionally, we introduce a Contrastive Enhancement (CE) process prior to MHM. In particular, by simply subtracting the similarities between support background and the query from the hypercorrelation, the subsequent MHM can acutely capture the embedding entanglement cues, thus suppressing erroneous correspondence for more accurate segmentation.

Overall, we summarize our key contributions as follows:

- Based on our preliminary analysis (Sec. III), we design a new, lightweight segmenter with BA, MVPG and a mask decoder, which contains only 5.6M parameters (5% of SAM’s) yet maintains strong performance. The framework, UINO-FSS, unifies SAM and DINOv2 within a single-encoder architecture and solely depends on meta-visual prompts without hyperparameters.
- We enhance the vanilla Meta-Visual Prompt Generator (MVPG) with the novel Mamba-HyperCorrelation module and contrastive enhancement. That processes 4D correlation with reduced embedding coupling.
- A family of compact UINO-FSS models on DINOv2 variations (DINOv2-Small, Base, Large) is trained and validated, proving the generalization of the framework.
- Our proposed method achieves State-of-the-Art (SOTA) performance, with dramatic improvements of 3.8% IoU on PASCAL-5ⁱ [5] and 4.1% on COCO-20ⁱ [26] benchmarks under the challenging 1-shot setting.

II. RELATED WORK

A. Semantic Segmentation

Semantic segmentation, which involves assigning a semantic label to each pixel, constitutes a fundamental task in computer vision. A key challenge in this area lies in the effective integration of global and local feature encoding. Early architectures such as UNet [27], [28] preserve local spatial details through skip connections, while subsequent methods used dilated convolutions [29]–[31] and multi-scale modules [32]–[34] to capture broader contextual information and better global semantics. Techniques such as [35] and [36] insert dual-attention and cross-attention, respectively, into convolutional backbones, further improving contextual reasoning. More recently, Vision Transformer (ViT)-based frameworks [37]–[39] combine the ViT encoder with a mask decoder, leading to a unified architecture. Unlike traditional methods that predict pixel labels independently, self-attention in the mask decoder allows object queries to perceive the others, facilitating global reasoning. Following this trend, SAM [22] incorporates prompt encoding and achieves strong class-agnostic segmentation via large-scale pretraining. While SAM excels in global boundary detection at the cost of local details, DINOv2 provides rich local features but lacks a powerful decoder, underscoring the ongoing efforts of unifying global and local cues.

B. Few-shot Semantic Segmentation

Instead of supervising on massive annotations, few-shot semantic segmentation aims to segment novel semantics using only a limited number of annotated samples. In this field, meta-learning has been widely employed to train general models via episodic learning. Early work [6] constructs class prototypes by applying masked average pooling (MAP) to support images, and segments query images by measuring pixel-wise distances to these prototypes in the metric space. To overcome the limitations of single prototype, [7]–[9], [11], [12], [40] represent each class with multiple prototypes, while [10] employs an additional independent encoder to process MAP features. PCNet [40] introduces a self-distillation mechanism to enable complementary learning between query and support prototypes, resulting in more accurate prototype representations. Since prototype-based methods are inherently limited by feature averaging, subsequent approaches [13]–[16], [41]–[43] explicitly build support-query feature aggregation modules to fully exploit the information in limited supports. Among them, [16] first calculates 4D correlation volume between the support and query image. For computational efficiency, this volume is decoupled into 2D similarity maps along the query and support dimensions, alternatively, and then processed with convolutions. Methods such as [13], [15], [18], [44]–[46] adopt support-query cross-attention mechanisms. CyCTR [13] consists of two transformers: a self-alignment block that aggregates contextual information within the query image, and a cross-alignment block that integrates pixel-level support features into the query features. Unlike [13], which applies self-attention only to query features, [46] applies self-attention to both support and query features and then uses cross-attention

to reorganize these features, generating prototypes for guiding segmentation. Based on support-query fusion, [47] performs region matching to produce context-aware prior masks. Other works [14], [15], [17], [42], [45] employ multi-layer features for matching. Among them, [15] applies knowledge distillation to enable lower-level correlation volumes learned from higher-level maps, capturing richer contextual information. Unlike these approaches, for support-query aggregation, we introduce a Mamba-based module enhanced by contrastive hypercorrelation. Building on Mamba’s computational efficiency and its dynamic, input-selective contextual processing capabilities, our method is shown to achieve more comprehensive and robust hypercorrelations for mask decoding.

C. Vision Foundation Models in Few-shot Segmentation

With the development of pre-trained visual models such as ViT [48], CLIP [21], SAM [22], and DINOv2 [20], Few-shot Semantic Segmentation (FSS) models [1], [3], [49] have achieved significant improvements on benchmark datasets. Particularly, [50] casts a CLIP on top of existing well-trained FSS networks, leading to further improvements. Among methods derived from SAM, the training-free method [1] generates point prompts using support-query similarity based on DINOv2 features, with dual-directional pruning. Inspired by [1], [2] enhances segmentation by building a graph on the generated masks. Other works, like [3], aim to learn prompt encoders to avoid complex hand-crafted procedures but still rely on both SAM and DINOv2, resulting in large memory footprints. In contrast, [25] bypasses SAM and trains a decoder directly on DINOv2 features. Compared with [25], while both methods demonstrate high efficiency, but our method achieves significantly superior performance. This primarily stems from the pivotal finding of feature alignment between DINOv2’s low-level features and SAM encoder’s outputs, which enables a superior decoder through embedding distillation. Furthermore, our approach is enhanced by an effective MVPG module that generates both sparse prompts and Mamba-based dense prompts for decoding.

III. PRELIMINARY

Since both DINOv2 and SAM are utilized for the few-shot segmentation task [1]–[3], the input images are passed through two separate image encoders to extract features independently. This results in a model with a large number of parameters and high inference time, making it less practical for real-world applications. To address this issue, we propose learning SAM’s feature distribution by introducing a small number of trainable parameters after DINOv2 encoder, enabling SAM’s powerful decoder on top of DINOv2. However, experimental results reveal significant distinctions between the features from these two models, as illustrated in Fig. 2. The distillation loss that aims to align the two kinds of features does not decrease. To this end, we compute self-similarities of features from DINOv2 and SAM’s encoders separately for analysis.

Given a feature representation $F \in \mathbb{R}^{H \times W \times C}$ obtained from the image encoder, we first reshape it into a two-

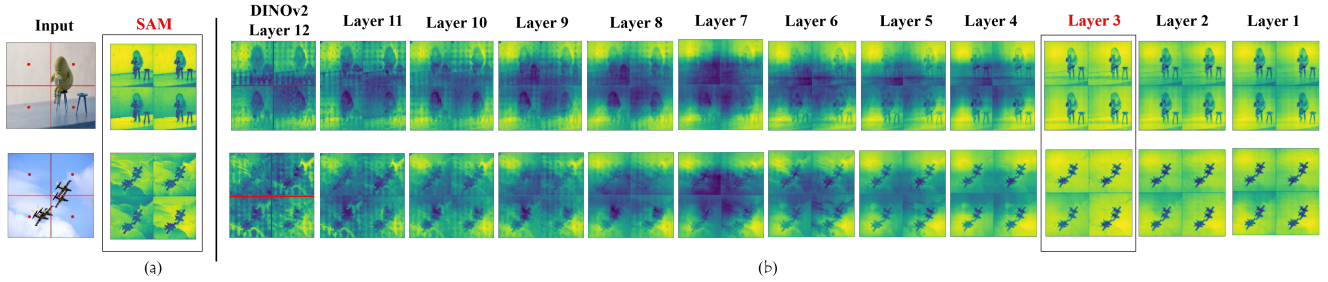


Fig. 2. **Analysis on the embeddings from DINOv2 and SAM.** We compute the self-similarity map (SSM) of feature vectors on red dots to analyze the embedding distribution of both models and visualize them in the figure. Here, (a) shows the SSM of features from the last layer of SAM’s encoder, while (b) displays the SSM of features from all layers of DINOv2-Base. Unlike SAM’s holistic semantic focus, DINOv2’s high-level embeddings concentrate on various local regions, offering richer representation. Despite this, we found that embeddings from DINOv2’s 3rd layer are most similar to SAM’s encoder embeddings. This observation enables efficient cross-model distillation for our lightweight segmenter.

dimensional matrix $F \in \mathbb{R}^{HW \times C}$, and then compute the cosine similarity after normalization, formulated as:

$$S_{ij} = \frac{F_i \cdot F_j}{\|F_i\| \|F_j\|}, \quad \forall i, j \in [1, HW], \quad (1)$$

where S_{ij} represents the similarity between feature vectors at positions i and j . For each position i , by computing its correlation with all positions in the image, we get a similarity map of size $H \times W$. Fig. 2 shows instances of the Self-Similarity Maps (SSM) on four anchor points.

As illustrated in Fig. 2, the self-similarity analysis reveals distinct characteristics between the representations of SAM and DINOv2. SAM’s features exhibit strong global characteristics, where each pixel can perceive semantic information across the entire image. In contrast, DINOv2’s features are more localized, with each pixel focusing primarily on the neighboring regions of the same semantics. *An interesting observation* is that DINOv2 can already capture holistic attention in its early-stage embeddings (Layer 3 in Fig. 2 (b)) but is trained to represent richer details in the high-level layers. **This suggests that a complete DINOv2 model is not strictly necessary for capturing SAM’s representation, and transferring knowledge from DINOv2’s early-stage features is practicable.** For DINOv2-Base, we utilize features from the 3rd layer, which are found to best match the distribution of SAM’s output embedding.

IV. APPROACH

A. Problem Definition

In the task of Few-Shot Semantic Segmentation (FSS), a dataset D is divided into a training set D_{train} and a test set D_{test} , with disjoint category sets, i.e., $C_{\text{train}} \cap C_{\text{test}} = \emptyset$, to ensure no class overlap between training and testing. The FSS model is first trained on the base classes from the training set and is then directly evaluated on the novel classes in the test set, without any additional training or fine-tuning. Specifically, given N support images and their corresponding pixel-wise masks for a novel class c , the FSS model aims to segment the pixels belonging to class c in a query image based on the support information. This process is referred to as N-shot segmentation.

B. Model Overview

In this work, we introduce a unified framework consisting of a DINOv2 encoder and a lightweight segmenter, as shown in Fig. 3. In the following, we will give an overview of both our architecture and the training strategy.

a) *The Architecture:* The unified UIINO-FSS comprises a frozen DINOv2’s encoder and a lightweight segmenter, as shown in Fig. 3. Inspired by SAM [22], the segmenter is designed to decode masks using both prompts and image features. Unlike SAM encoding points/boxes, our segmenter directly generates visual prompts. In particular, the segmenter incorporates three components: a Bottleneck Adapter (BA), a Meta-Visual Prompt Generator (MVPG), and a mask decoder. The BA imports the low-level features from the frozen encoder and adapts them into embeddings suited for boundary localization and semantic segmentation. The MVPG generates semantic-aware visual prompts and Mamba-based dense prompts using features from the encoder’s last layer.¹ Inheriting SAM’s decoder architecture, our mask decoder integrates prompts with image features generated by the bottleneck adapter to produce the final mask.

b) *Training Strategy:* Our training consists of two stages, i.e., the embedding distillation and training for mask decoding. During both training stages, the DINOv2 encoder is frozen and only parts of our segmenter are trained. In the first stage, we train only the adapter with a Mean-Square-Error (MSE) loss to align the embeddings from SAM and the 3rd layer of DINOv2, without being aware of the downstream task. In the second stage, with the DINOv2’s encoder and the adapter frozen, the remaining components of the segmenter, i.e., the MVPG and mask decoder, are further optimized via meta learning for few-shot semantic segmentation, where the decoder is initialized with SAM’s parameters. By integrating knowledge distillation with an effective decoder initialization, our method successfully combines the strengths of DINOv2 and SAM.

C. Hierarchical Distillation for Embedding Alignment

Based on our observation in Sec. III, we directly leverage the 3rd-layer features of DINOv2-Base and train a lightweight

¹The semantic-aware prompt and Mamba-based dense prompt work as sparse and dense prompts, respectively, as used in SAM.

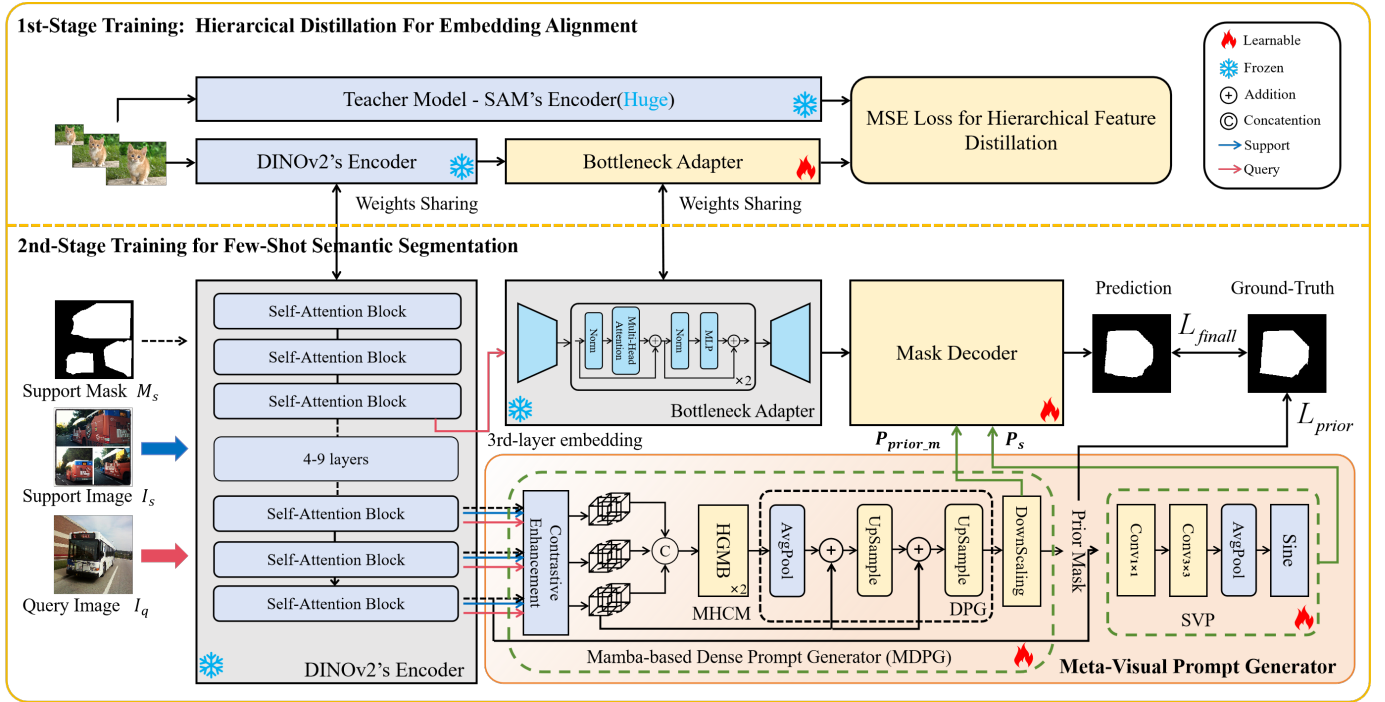


Fig. 3. **The proposed UINO-FSS architecture.** Our architecture consists of a DINOv2 encoder and a lightweight segmenter that includes a bottleneck adapter (BA), a Meta-Visual Prompt Generator (MVPG) and a mask decoder. Upper part is the coarse-to-fine cross-model distillation procedure, with only the adapter trainable for feature matching. Below is the overall architecture of our few-shot semantic segmentation model. Our MVPG includes two modules for the Semantic-aware Visual Prompts (SVP) and the Mamba-based dense prompts, respectively.

adapter with a bottleneck structure to align its embeddings with SAM. During embedding distillation, SAM-huge’s encoder serves as the teacher, while DINOv2’s 1-3 layers together with the trainable adapter, constitute the student. Only the adapter’s parameters are updated during the process.

1) *The Bottleneck Adapter:* To maintain a lightweight design, we build a bottleneck-structured adapter to efficiently transfer embedding features. As shown in Fig. 3, the adapter takes features from DINOv2-Base’s low-level layer l_{low} ($l_{low}=3$) as input, denoted as $F^{low} \in \mathbb{R}^{H \times W \times C}$, and transforms them into $F^{ba} \in \mathbb{R}^{H \times W \times C_{sam}}$ to align with the feature dimension of SAM encoder’s last layer, where $C = 768$, $C_{sam} = 256$, H and W are the height and width of the feature map, respectively². Specifically, we first apply a sequence of convolutions to reduce the channel dimension from C to a lower intermediate dimension C' ($C' = 128$), in order to compress redundant information and reduce computation³. We then employ two self-attention blocks to enhance the feature representation, followed by a pointwise convolution that increases the channel dimension to the target dimension C_{sam} . The self-attention blocks adopt the standard Transformer structure, with $Q, K, V \in \mathbb{R}^{C' \times C'}$ and the inner-layer dimension of feed-forward network (FFN) being 512, enabling long-range dependency modeling across channels. For other models within the DINOv2 family, i.e., DINOv2-Small/Large, we employ a similar design to align

²Given input image size 518×518 , we get feature dimensions H and W both being 37.

³Convolutions with sizes of $1 \times 1 \times 768 \times 256$, $3 \times 3 \times 256 \times 256$, and $1 \times 1 \times 256 \times 128$ are applied here for dimension reduction.

their low-level features with the output of the SAM encoder⁴.

2) *Cross-model Distillation from Coarse to Fine:* Given that SAM’s features capture holistic semantic information, we design a hierarchical distillation procedure to progressively align features from coarse to fine across multiple stages. Specifically, we start training with a low input resolution of 126×126 , and at each distillation stage, the resolution is doubled for further training. This iterative process is conducted twice, eventually reaching a resolution of 518×518 , which corresponds to the input size used by DINOv2. Through this progressive training strategy, our model gradually fits the feature distribution of SAM and effectively replaces its image encoder. In practice, due to SAM’s holistic-embedding nature, a coarse-to-fine distillation over hierarchical resolutions proves critical, as direct distillation on fine resolutions leads to slow convergence. Let’s denote the output of the bottleneck adapter as F^{ba} , and the final-layer features from the encoder of SAM-ViT-Huge as F^{sam} . By minimizing the mean squared error (MSE) between F^{ba} and F^{sam} , we encourage our model to match the output distribution of SAM. Notably, only 1% of SAM’s training images are used throughout the distillation process.

D. Meta-Visual Prompt Generator

To enable prompt-assistant decoding, this work generates two kinds of prompts, i.e., the semantic-aware visual prompt and Mamba-based dense prompts.

⁴For DINOv2-Small/Large, we choose comparable low-level layers, i.e., $l_{low} = 2$ and 4, respectively.

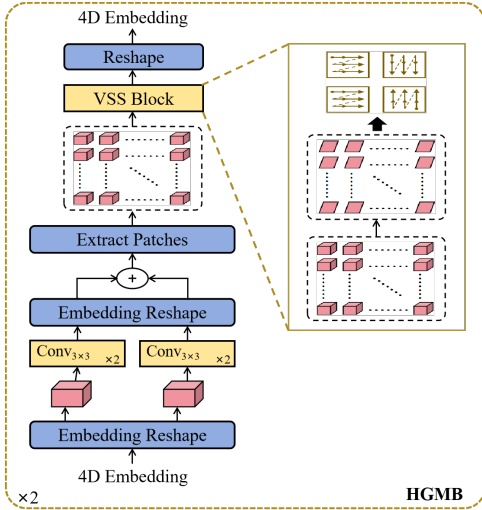


Fig. 4. Network structure for the Mamba-HyperCorrelation Module (MHCM). MHCM stacks two Hierarchical Global Modeling Blocks (HGMB), which process 4D volumetric correlation while maintaining high efficiency.

1) *Semantic-aware Visual Prompts*: To provide Semantic-aware Visual Prompts (SVP), we directly generate embedding vectors from the support features. Specifically, we first perform dimension reduction on the last layer feature map $F \in \mathbb{R}^{H_s \times W_s \times C}$ of DINOv2 through convolutional layers to obtain $F' \in \mathbb{R}^{H_s \times W_s \times C_{sam}}$,

$$F' = \mathcal{F}_{\text{conv}}(F), \quad (2)$$

where $\mathcal{F}_{\text{conv}}$ denotes a convolutional block composed of a 1×1 and 3×3 convolution, each followed by layer normalization. We then perform masked average pooling (MAP) on F' to extract the foreground class prototypes. To align with SAM's positional encoding, we further encode these prototypes using the sine function to obtain the sparse prompts $P_s \in \mathbb{R}^{1 \times C_{sam}}$,

$$P_s = \mathcal{F}_{\text{sine}}(\mathcal{F}_{\text{MAP}}(F')). \quad (3)$$

The semantic-aware visual prompt P_s matches the dimension of SAM's sparse prompt for direct use with its decoder.

2) *Mamba-based Dense Prompt Generator*: By integrating the SVP and a vanilla 2D similarity map between query features and support prototypes, we can already construct a strong framework with negligible parameters. To further improve the framework while maintaining its lightweight structure, we introduce the Mamba-based dense prompt generator, featuring the contrastive enhancement on similarity volumes, a Mamba-HyperCorrelation Module (MHCM), and a module for dense prompt generation.

a) *Contrastive Enhancement*: This module is proposed to inject contrastive embeddings into correlation volumes, to enhance subsequent hypercorrelation modeling. To this end, we extract features from the last three layers ($l = 3$) of the DINOv2 encoder and embed the query's similarities to both the support's foreground and background regions.

Specifically, we first perform an element-wise multiplication between the support mask, $M_s \in \{0, 1\}^{H_s \times W_s}$, and the

support features, achieving the masked foreground features F_s^{fg} and background features F_s^{bg} as below,

$$F_s^{fg} = M_s \odot F_s, \quad F_s^{bg} = (1 - M_s) \odot F_s. \quad (4)$$

For each selected layer, we compute two correlation volumes between the query features and the masked support features:

$$\mathcal{V}_{fg}^{(i)}{}_{h_q, w_q, h_s, w_s} = \frac{\langle F_q^{(i)}(h_q, w_q), F_s^{fg(i)}(h_s, w_s) \rangle}{\|F_q^{(i)}(h_q, w_q)\| \cdot \|F_s^{fg(i)}(h_s, w_s)\|}, \quad (5)$$

$$\mathcal{V}_{bg}^{(i)}{}_{h_q, w_q, h_s, w_s} = \frac{\langle F_q^{(i)}(h_q, w_q), F_s^{bg(i)}(h_s, w_s) \rangle}{\|F_q^{(i)}(h_q, w_q)\| \cdot \|F_s^{bg(i)}(h_s, w_s)\|}. \quad (6)$$

where $\mathcal{V}_{fg}^{(i)}$ and $\mathcal{V}_{bg}^{(i)} \in \mathbb{R}^{H_q \times W_q \times H_s \times W_s}$ denote the correlation volumes derived from the i -th layer, computed using the foreground and background support features respectively. To suppress the inherent background noise of the ViT backbone, we directly subtract the background correlation volume from the foreground correlation volume on each of the last l layers and concatenate the results. This process can be formulated as below,

$$\mathcal{V}^{(i)} = \mathcal{V}_{fg}^{(i)} - \mathcal{V}_{bg}^{(i)}. \quad (7)$$

$$\mathcal{V} = \mathcal{V}^{(L-l+1)} \oplus \mathcal{V}^{(L-l+2)} \oplus \dots \oplus \mathcal{V}^{(L)}, \quad (8)$$

where L denotes the overall number of layers in DINOv2 image encoder, the symbol \oplus indicates concatenation along an additional dimension. $\mathcal{V} \in \mathbb{R}^{l \times H_q \times W_q \times H_s \times W_s}$ encodes the query-to-support matching information across multiple layers.

b) *Mamba-HyperCorrelation Module*: To avoid the high cost of 4D convolution, prior work [16] reshapes the volume \mathcal{V} into forms $\mathcal{V}_a \in \mathbb{R}^{(H_s \cdot W_s) \times l \times H_q \times W_q}$ and $\mathcal{V}_b \in \mathbb{R}^{(H_q \cdot W_q) \times l \times H_s \times W_s}$, which can then be processed with 2D convolutions independently in batch⁵. This strategy, however, lacks global semantic modeling, limiting its ability to correct regional misalignments. To address this, we introduce the Hierarchical Global Modeling Block (HGMB) that processes true 4D volumes while maintaining high efficiency. By stacking HGMBs, we construct the Mamba-HyperCorrelation Module.

Specifically, the HGMB integrates VMamba [51], alternating between local and global modeling by stacking a convolution block and a patch-wise visual state space (VSS) block. Its structure is shown in Fig. 4. In detail, (1) we first apply a 3×3 convolution to locally process the 2D correlations \mathcal{V}_a and \mathcal{V}_b to increase the channel dimensionality. The results are then reshaped back to the shape of \mathcal{V} and summed together to form a new correlation volume, $\hat{\mathcal{V}} \in \mathbb{R}^{l \times H_q \times W_q \times H_s \times W_s}$, which integrates interactions within the support and query neighbors; (2) Given the augmented correlation volume $\hat{\mathcal{V}}$, we partition it into non-overlapping local blocks within the 4D space. This operation reshapes the volume $\hat{\mathcal{V}}$ into $\mathbb{R}^{l \times N \times k_q \times k_q \times k_s \times k_s}$, where k_q and k_s is partition sizes along support and query dimensions, and N is the number of local blocks⁶. Subsequently, we flatten the query and support spatial dimensions of each block, transforming it into a 2D patch. This yields the representation $\mathcal{V}_p \in \mathbb{R}^{l \times N \times k_q \times k_q \times k_s \times k_s}$. To suppress the

⁵Here, the first dimension always serves as batch dimension.

⁶ $N = \frac{H_q}{k_q} \times \frac{W_q}{k_q} \times \frac{H_s}{k_s} \times \frac{W_s}{k_s}$.

potential interference caused by noisy or abnormal correlations within these local blocks, we incorporate a Visual State Space (VSS) module to process each 2D patch. Finally, the processed correlation volumes are reshaped back to their original 4D structure, yielding $\tilde{\mathcal{V}}'$ formulated as below,

$$\tilde{\mathcal{V}}' = \text{Reshape}(\mathcal{F}_{\text{vss}}(\mathcal{V}_p)). \quad (9)$$

In Eq. 9, the VSS module, denoted by \mathcal{F}_{vss} , processes each 2D patch by traversing and modeling its structure through a structured state space model (SSM). This formulation enables efficient capture of long-range dependencies within the patch while suppressing noise interference, all with linear computational complexity relative to the sequence length.

c) *Dense Prompt Generation*: To generate the dense prompt, we project the refined correlation volume to the decoder’s input dimension. For stability, a residual connection is introduced to combine the refined volume $\tilde{\mathcal{V}}'$ with the raw 4D foreground correlation $\mathcal{V}_{fg}^{(L)}$ from Eq. 5, which encodes the query-support similarity from DINOv2’s last layer. Specifically, we first average $\mathcal{V}_{fg}^{(L)}$ and $\tilde{\mathcal{V}}'$ along the last two support dimensions, reducing them to 2D representations with 1 and l' channels respectively, which are then summed up with broadcasting. This operation is formulated as follows,

$$\mathcal{V}_{2d} = \mathcal{F}_{\text{AvgPool}}(\mathcal{V}_{fg}^{(L)}) + \mathcal{F}_{\text{AvgPool}}(\tilde{\mathcal{V}}'). \quad (10)$$

Next, \mathcal{V}_{2d} is upsampled and further projected into a prior mask $P_{\text{prior_m}} \in \mathbb{R}^{1 \times H'_q \times W'_q}$, where H'_q and W'_q denotes the final mask size. This prior mask, when input to the prompt encoder, can provide a dense prompt to guide the mask decoder. The process is as below:

$$P_{\text{prior_m}} = \mathcal{F}_{\text{Proj}}(\text{Upsample}(\mathcal{V}_{2d})), \quad (11)$$

where $\text{Upsample}(\cdot)$ denotes the upsampling operation and $\mathcal{F}_{\text{Proj}}(\cdot)$ employs a convolution followed by a sigmoid operation to convert 2D features into a mask probability map.

E. Mask Decoding via Meta-Visual Prompting

Given query image features from bottleneck adapter and prompts from the meta-visual prompt generator, the decoder predicts masks corresponding to the support class. To this end, the mask decoder is first initialized via parameters from the pre-trained mask decoder of SAM-ViT-Huge, and then trained via an episodic training strategy. This training strategy is widely used in meta-learning to simulate the inference process of few-shot segmentation, enabling effective generalization to unseen classes. Specifically, we construct each image batch via several support-query pairs following [15] and learn to predict masks for the current support class. It is important to note that during episodic training, we train exclusively on the base classes without involving the novel classes. The Dice Loss and BCE Loss are computed separately for the prior mask $P_{\text{prior_m}}$ and the final prediction P_m against the ground truth mask M_q . Particularly, the loss functions are defined as:

$$\mathcal{L}_{\text{prior}} = \mathcal{L}_{\text{Dice}}(P_{\text{prior_m}}, M_q) + \mathcal{L}_{\text{BCE}}(P_{\text{prior_m}}, M_q), \quad (12)$$

$$\mathcal{L}_{\text{final}} = \mathcal{L}_{\text{Dice}}(P_m, M_q) + \mathcal{L}_{\text{BCE}}(P_m, M_q), \quad (13)$$

$$\mathcal{L} = \mathcal{L}_{\text{prior}} + \mathcal{L}_{\text{final}}, \quad (14)$$

where $\mathcal{L}_{\text{Dice}}(\cdot)$ and $\mathcal{L}_{\text{BCE}}(\cdot)$ represent the Dice Loss and Binary Cross-Entropy (BCE) Loss, respectively.

V. EXPERIMENTS

A. Datasets and Evaluation Metrics

To evaluate the effectiveness of our proposed method, we conducted extensive experiments on two widely recognized benchmark datasets within the Few-Shot Segmentation (FSS) setting: PASCAL-5ⁱ [5] and COCO-20ⁱ [26]. The PASCAL-5ⁱ dataset, derived from PASCAL VOC 2012 [52], is augmented with additional annotations from SDS [53] and consists of 20 object classes. The COCO-20ⁱ dataset, constructed from MSCOCO [54], presents a more challenging setting as it includes 80 classes. For task partitioning, both PASCAL-5ⁱ and COCO-20ⁱ follow the standard cross-validation protocol, where all categories are divided into several non-overlapping folds. Each fold is used in turn as the test set, while the remaining categories serve as the training set, ensuring a fair evaluation of the model’s generalization ability across different categories. All experiments are conducted under both the 1-shot and 5-shot settings to investigate the model’s performance using varying amounts of support images. In addition, no further finetuning on the novel set is conducted. Furthermore, we conduct an out-of-distribution evaluation on FSS-1000 [55], a dataset specifically designed for FSS containing 1k classes. For evaluation, we adopt the standard mean Intersection over Union (mIoU) across various classes, i.e., $\text{mIoU} = \frac{1}{n} \sum_{i=1}^n \text{IoU}_i$, as the metric, where n is the number of test cases.

B. Implementation Details

The lightweight Bottleneck Adapter (BA) is trained on 1% of the SA-1B dataset [22] with three stages. In each stage, we train the model with 15 epochs, using an image size of 126×126 , 252×252 , and 518×518 , respectively. In the first two stages, the model is trained on 2 NVIDIA RTX A6000, and in the last stage on 4 RTX A6000 GPUs, with batch size 8. The model is optimized using the AdamW optimizer with an initial learning rate of $1e-3$ and a weight decay of $5e-4$.

While training for mask decoding and few-shot segmentation, all experiments on the PASCAL-5ⁱ [5] and COCO-20ⁱ [26] datasets were conducted with images of size 518×518 , using the frozen encoder from the DINOv2 pre-trained model ViT-B/14 to extract features. To ensure fair comparisons, we followed the same data augmentation and optimization settings as in [15]. In particular, images were augmented with random cropping, scaling, rotation, blur, and horizontal flipping, while the learning rate was gradually reduced using a polynomial decay schedule. AdamW was used as the optimizer with an initial learning rate of 0.001 and a weight decay of 5×10^{-4} , and the batch size was set to 8 for both datasets.

C. Comparison with State-of-the-Art Methods

1) *Few-shot Segmentation Performance*: In Tab. I and II, we compare our method with prior works categorized by

TABLE I
PERFORMANCE COMPARISONS ON PASCAL-5ⁱ UNDER 1-SHOT AND 5-SHOT SETTINGS. RESULTS IN BOLD INDICATE THE BEST PERFORMANCE, AND RESULTS WITH UNDERLINING REPRESENT THE SECOND-BEST PERFORMANCE.

Method	Backbone	1-shot					5-shot				
		Fold0	Fold1	Fold2	Fold3	Mean	Fold0	Fold1	Fold2	Fold3	Mean
BAM <i>CVPR'22</i> [56]	ResNet50	69.0	73.6	67.6	61.1	67.8	70.6	75.1	70.8	67.2	70.9
HDMNet <i>CVPR'23</i> [15]		71.0	75.4	68.9	62.1	69.4	71.3	76.2	71.3	68.5	71.8
AENet <i>ECCV'24</i> [57]		71.3	75.9	68.6	65.4	70.3	73.9	77.8	73.3	72.0	74.2
OCNet <i>ICCV'25</i> [58]		73.5	75.9	71.1	64.9	71.4	75.9	77.1	74.1	70.9	74.5
MSI <i>ICCV'23</i> [43]		73.1	73.9	64.7	68.8	70.1	73.6	76.1	68.0	71.3	72.2
SCCAN <i>ICCV'23</i> [18]	ResNet101	70.9	73.9	66.8	61.7	68.3	73.1	76.4	70.3	66.1	71.5
ABCB <i>CVPR'24</i> [59]		73.0	76.0	69.7	69.2	72.0	74.8	78.5	73.6	72.6	74.9
Matcher <i>ICLR'24</i> [1]	DINOv2-L, SAM-H	67.7	70.7	66.9	67.0	68.1	71.4	77.5	74.1	72.8	74.0
GF-SAM <i>NeurIPS'24</i> [2]		71.1	75.7	69.2	<u>73.3</u>	72.1	<u>81.5</u>	<u>86.3</u>	79.7	<u>82.9</u>	<u>82.6</u>
VRP-SAM <i>CVPR'24</i> [3]	ResNet50, SAM-H	73.9	78.3	70.6	65.0	71.9	-	-	-	-	-
FCP <i>AAAI'25</i> [60]		74.9	77.4	71.8	68.8	73.2	77.2	78.8	72.2	67.7	74.0
PI-CLIP <i>CVPR'24</i> [50]	ResNet50, CLIP	<u>76.4</u>	83.5	<u>74.7</u>	72.8	<u>76.8</u>	76.7	83.8	75.2	73.2	77.2
Ours	DINOv2-B	80.7	<u>83.2</u>	77.8	80.5	80.6	84.4	87.3	<u>79.0</u>	85.5	84.1

TABLE II
PERFORMANCE COMPARISONS ON COCO-20ⁱ UNDER 1-SHOT AND 5-SHOT SETTINGS. OUR METHOD CONSISTENTLY ACHIEVES THE BEST PERFORMANCE, OUTPERFORMING OTHER APPROACHES BASED ON DINOv2-BASE (DINOv2-B) AS WELL AS HEAVIER ARCHITECTURES COMBINING DINOv2-LARGE (DINOv2-L) AND SAM-ViT-H (SAM-H).

Method	Backbone	1-shot					5-shot				
		Fold0	Fold1	Fold2	Fold3	Mean	Fold0	Fold1	Fold2	Fold3	Mean
BAM <i>CVPR'22</i> [56]	ResNet50	43.4	50.6	47.5	43.4	46.2	49.3	54.2	51.6	49.6	51.2
HDMNet <i>CVPR'23</i> [15]		43.8	55.3	51.6	49.4	50.0	50.6	61.6	55.7	56.0	56.0
AENet <i>ECCV'24</i> [57]		45.4	57.1	52.6	50.0	51.3	52.7	62.6	56.8	56.1	57.1
OCNet <i>ICCV'25</i> [58]		45.9	56.9	52.9	50.4	51.5	52.7	63.1	57.4	54.8	57.0
MSI <i>ICCV'23</i> [43]		44.8	54.2	52.3	48.0	49.8	49.3	58.0	56.1	52.7	54.0
SCCAN <i>ICCV'23</i> [18]	ResNet101	42.6	51.4	50.0	48.8	48.2	49.4	61.7	61.9	55.0	57.0
ABCB <i>CVPR'24</i> [59]		46.0	56.3	54.3	51.3	51.5	51.6	63.5	62.8	57.2	58.8
Matcher <i>ICLR'24</i> [1]	DINOv2-L, SAM-H	52.7	53.5	52.6	52.1	52.7	60.1	62.7	60.9	59.2	60.7
GF-SAM <i>NeurIPS'24</i> [2]		56.6	61.4	59.6	57.1	58.7	67.1	69.4	<u>66.0</u>	<u>64.8</u>	<u>66.8</u>
FCP <i>AAAI'25</i> [60]	ResNet50, SAM-H	46.4	56.4	55.3	51.8	52.5	52.6	63.3	59.8	56.1	58.0
VRP-SAM <i>CVPR'24</i> [3]	DINOv2-B, SAM-H	<u>56.8</u>	61.0	<u>64.2</u>	<u>59.7</u>	<u>60.4</u>	-	-	-	-	-
SEGIC <i>ECCV'24</i> [25]	DINOv2-B, CLIP	55.8	54.7	52.4	51.4	53.6	-	-	-	-	-
PI-CLIP <i>CVPR'24</i> [50]	ResNet50, CLIP	49.3	<u>65.7</u>	55.8	56.3	56.8	56.4	66.2	55.9	58.0	59.1
Ours	DINOv2-B	62.2	66.0	65.5	64.4	64.5	<u>66.6</u>	73.3	70.9	68.1	69.7

TABLE III
PERFORMANCE ON FSS-1000 UNDER ONE-SHOT SETTING.

Metric	Painter [61]	SegGPT [62]	PerSAM [24]	PerSAM-F [22]	SegIC [25]	Ours
mIoU	61.7	85.6	71.2	75.6	<u>86.8</u>	89.0

their backbones. Among foundation model-based approaches, Matcher [1] and GF-SAM [2] are training-free but rely on large pre-trained models, while others—such as VPR-SAM [3], FCP [60], PI-CLIP [50], and SEGIC [25]—ever undergo supervised training on the target task, i.e., few-shot semantic

segmentation, to attain stronger performance. **Our method gains dramatic improvements over the previous methods with fewer model parameters** (as shown in Tab. IV) on both PASCAL-5ⁱ and COCO-20ⁱ datasets, thanks to the unified architecture and enhanced meta-visual prompt generator.

Specifically, on the PASCAL-5ⁱ dataset, our method outperforms PI-CLIP and GF-SAM by 3.8% and 1.5% in mIoU, which held the previous state-of-the-art in the 1-shot and 5-shot settings, respectively. The COCO-20ⁱ dataset presents a more challenging benchmark due to its greater number of categories and higher diversity in object sizes. Even under these conditions, our approach maintains consistently superior performance, exceeding the 1-shot SOTA (VRP-SAM) by

TABLE IV
COMPARISON OF THE NUMBER OF TRAINABLE/TOTAL PARAMETERS AND mIoU ON COCO-20ⁱ UNDER 1-SHOT SETTING. UINO-FSS-COMP(*) REFERS TO OUR COMPACT MODEL WITHOUT DECODER TRAINING.

Method	Train Params	Total Params	mIoU
Matcher	0	945.5M	52.7
GF-SAM	0	945.5M	58.7
FCP	2.9M	667.6M	52.5
SEGIC	5.4M	432.8M	53.6
VRP-SAM (ResNet50)	1.6M	664.8M	53.9
UINO-FSS-Comp*	0.07M	92.0M	57.2
UINO-FSS-Comp	4.1M	92.0M	<u>59.6</u>
UINO-FSS	4.6M	<u>92.5M</u>	64.5

TABLE V
ABLATION STUDY RESULTS ON COCO-20ⁱ UNDER THE ONE-SHOT SETTING. HERE, WE DENOTE BA AS THE BOTTLENECK ADAPTER, PCS THE PROTOTYPE-BASED COSINE SIMILARITY, SVP THE SEMANTIC-AWARE VISUAL PROMPT, MHCM THE MAMBA-HYPERCORRELATION MODULE AND CE THE CONTRASTIVE ENHANCEMENT MODULE.

BA	PCS	SVP	MHCM	CE	mIoU (%)
✓	✓				58.2
✓	✓	✓			59.6
✓	✓	✓	✓		62.3
✓	✓	✓	✓	✓	64.5

4.1% and the 5-shot SOTA (GF-SAM) by 2.9% in mIoU. It is worth noting that the compared methods are strong benchmarks utilizing large foundation models. Particularly, our model uses a DINOv2-Base (ViT-B/14) backbone, while VRP-SAM uses additional SAM-ViT-Huge (SAM-H) and GF-SAM combines large DINOv2 with SAM-H. Our superior performance with more efficient architecture fully demonstrates the effectiveness of our design compared to existing methods.

2) *Out-of-Distribution Performance*: To evaluate the generalization ability of our model, we conduct one-shot assessments on the FSS-1000. Here, FSS-1000 is selected for its task alignment with ours, i.e., segmenting all regions of the support class rather than distinguishing instances. To assess the generality of our approach, we directly applied a model pretrained on the COCO-20ⁱ base set to FSS-1000 without any additional fine-tuning. This setting is specifically challenging due to the significant domain shifts between the datasets. The results are presented in Tab. III. As shown in the table, our model surpasses SEGIC [25] and PerSAM-F[†] [24], demonstrating outstanding transferability.

3) *Model Complexity Analysis*: Once the distilled model (DINOv2-B & Bottleneck Adapter) is obtained in the first training stage, it can be frozen and serve as a foundational feature extractor. Based on this, we provide a series of models with incremental trainable parameters: the UINO-FSS-Comp*, UINO-FSS-Comp, and the full UINO-FSS. The UINO-FSS-Comp* retains the same architecture as UINO-FSS but replaces the Mamba-based Dense Prompt Generator (MDPG) with a parameter-free, vanilla dense prompt, which calculates

TABLE VI
MORE ABLATION STUDIES ON HGMB UNDER THE ONE-SHOT SETTING, WHERE [†] DENOTES THE ABBREVIATION FOR CENTER-PIVOT 4D CONVOLUTION. WE REPLACE HGMB WITH CP4D CONV, KEEPING ALL OTHER MODULES UNCHANGED. OUR HGMB DEMONSTRATES SIGNIFICANT IMPROVEMENTS OVER CP4D CONV ON BOTH COCO-20ⁱ AND PASCAL-5ⁱ.

Dataset	Method	Fold0	Fold1	Fold2	Fold3	mIoU
COCO-20 ⁱ	UINO-FSS w/ CP4D Conv [†] [16]	61.9	65.9	64.9	63.1	64.0
	UINO-FSS	62.2	66.0	65.5	64.4	64.5
PASCAL-5 ⁱ	UINO-FSS w/ CP4D Conv [†] [16]	79.6	82.9	77.0	79.3	79.7
	UINO-FSS	80.7	83.2	77.8	80.5	80.6

support prototype-based cosine similarity (PCS) to the query features. As a result, the model only introduces a few additional convolutions for semantic-aware visual prompts. With its decoder frozen, the total number of trainable parameters is only 0.07M. Based on UINO-FSS-Comp*, the UINO-FSS-Comp variant additionally trains the decoder, yielding a model with 4.1M total trainable parameters. UINO-FSS incorporates MDPG at a cost of merely 0.5M additional parameters, of which the Mamba-based Hyper-Correlation Module (MHCM) accounts for only 0.18M. As shown in Tab. IV, on COCO-20ⁱ, UINO-FSS achieves the best mIoU among all compared methods while maintaining the least total parameters and only a small amount of trainable parameters. Even the UINO-FSS-Comp* can match the performance of GF-SAM with faster inference, and surpass VRP-SAM (ResNet50)⁷ with +3.6% mIoU and fewer trainable parameters. Even though our full model introduces limited trainable parameters, its dramatically superior FSS performance, high efficiency, and significantly fewer parameters (only 10% of GF-SAM), solidly demonstrated its value for FSS.

D. Ablation Study

To evaluate our model’s effectiveness, we conducted thorough ablation studies on COCO-20ⁱ under one-shot setting. To maintain experimental consistency, we selected DINOv2-Base as the image encoder and trained the mask decoder in all the ablation studies.

1) *Effectiveness of the Proposed Modules*: We incrementally adds the proposed modules to the framework and have proved their effectiveness and contributions as shown in Tab. V. Particularly, the BA+PCS, a framework leveraging distilled features from Bottleneck Adapter (BA) as the image embedding and the Prototype-based Cosine Similarity (PCS) as dense prompt, forms a basic baseline. It gets 58.2% mIoU in one-shot setting, with even 5.5% performance gains over the strong benchmark of Matcher [1]. This result, again, proves the effectiveness of the unified framework. An interesting observation is that, using initial sparse prompt embedding from SAM’s prompt encoder does not affect the performance, while replacing it with the Semantic-aware Visual Prompts (SVP) leads to 1.4% mIoU improvement, as shown by

⁷For VRP-SAM, since the model parameters are only available for its variant with ResNet-50 and SAM-H backbones, here we report the performance (53.9 mIoU) and time complexity of this variant in our comparison.

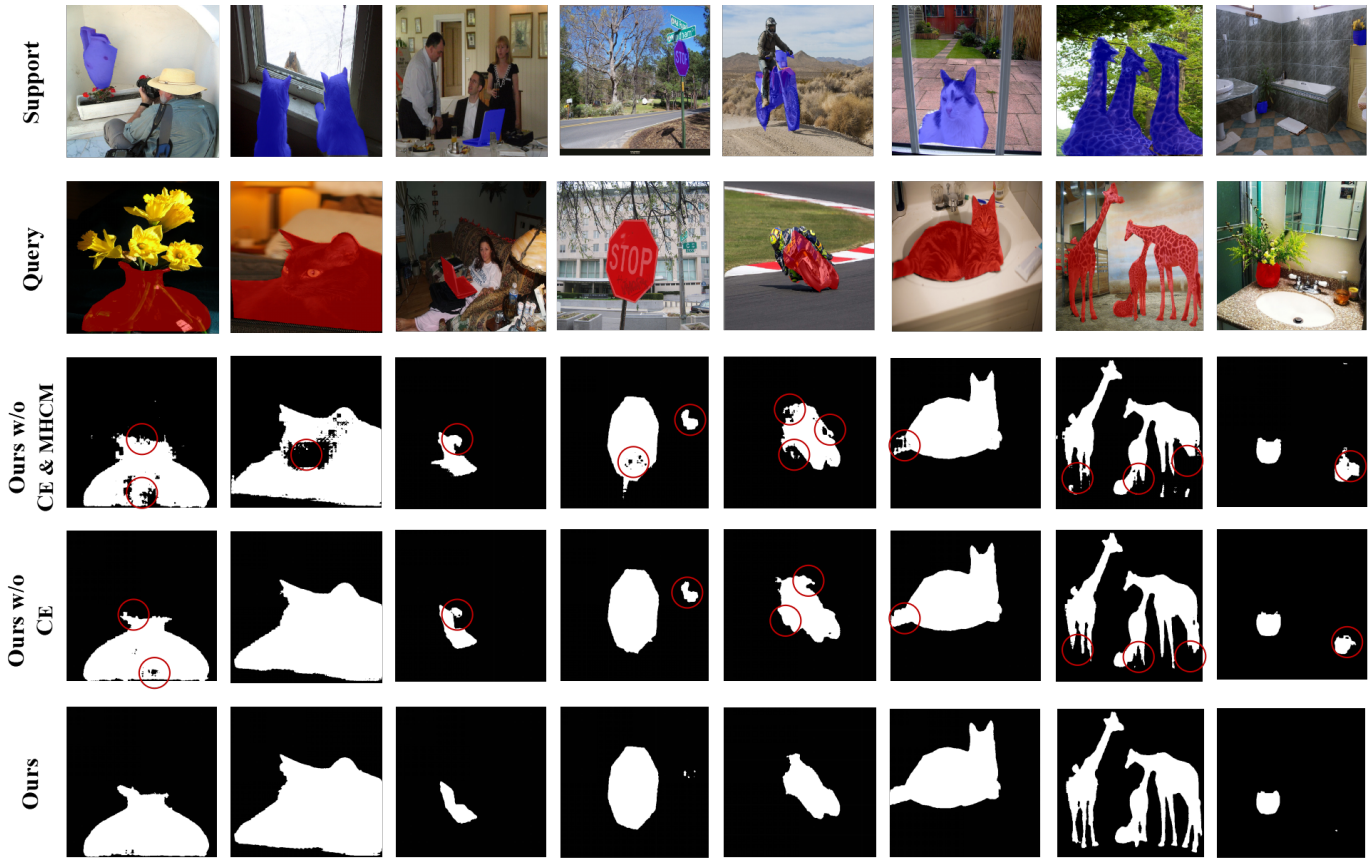


Fig. 5. **Qualitative results of UINO-FSS on COCO-20ⁱ under the one-shot setting.** From top to bottom in each row are the support image with its corresponding mask, the query image with ground-truth annotation, the output of UINO-FSS without CE and MHCM modules, the output of UINO-FSS without CE, and the output of the complete UINO-FSS model. Red circles indicate inaccurate segmentation.

BA+SVP+PCS. Upon it, the Mamba-based HyperCorrelation Module (MHCM) gets a dramatic improvement of 3.1% mIoU and the Contrastive Enhancement (CE) further boosts performance with 2.2% enhancement. To further validate MHCM, we replace it with the Center-pivot 4D convolution (CP4D Conv) module, a convolutional hypercorrelation implementation by [16]. As shown in Tab. VI, MHCM consistently surpasses CP4D Conv on PASCAL-5ⁱ and COCO-20ⁱ. Note that, since the unified framework already established a strong baseline with *BA+SVP+CE*, the additional gains produced by the lightweight MHCM are substantial and non-trivial.

In addition, we visualize the segmentation results in Fig. 5. We can see that the framework without CE and MHCM can already produce basically accurate segmentation, but the predicted masks involve holes, missing details and wrongly segmented backgrounds. The MHCM that models neighboring correlations in 4D space effectively blends the segmentation with enhanced details. The foreground/background contrastive enhancement in 4D correlation volume further removes wrongly segmented regions on backgrounds.

2) *Effectiveness of the Hierarchical Distillation:* To demonstrate the essential role of hierarchical distillation, here we re-train the compact UINO-FSS with distillation disabled. Specifically, we directly train the bottleneck adapter for few-shot semantic segmentation, with no feature alignment to SAM’s encoder. As shown in Tab. VII, eliminating distillation

TABLE VII
MORE STUDIES ON CROSS-MODEL DISTILLATION FROM COARSE TO FINE.

Method	Fold0	Fold1	Fold2	Fold3	mIoU
UINO-FSS-Comp w/o distillation	50.5	55.2	53.5	52.1	52.8
UINO-FSS-Comp	55.5	63.8	59.4	59.5	59.6

TABLE VIII
PERFORMANCE COMPARISON OF OUR COMPACT MODEL WITH DIFFERENT DINOv2 BACKBONES (SMALL/BASE/LARGE) ON COCO-20ⁱ UNDER 1-SHOT SETTING.

Method	Fold0	Fold1	Fold2	Fold3	mIoU
UINO-FSS-Comp w/ DINOv2-Small	49.2	58.5	55.3	54.3	54.3
UINO-FSS-Comp w/ DINOv2-Base	55.5	63.8	59.4	59.5	59.6
UINO-FSS-Comp w/ DINOv2-Large	57.6	63.8	61.6	59.9	60.7

results in a sharp 6.8% mIoU decline under the one-shot setting. The resulting 52.8% mIoU is virtually comparable to SEGIC’s mIoU of 53.6%, that’s a baseline training the mask decoder atop a frozen DINOv2 encoder. This outcome strongly affirms the necessity of incorporating knowledge distillation and feature alignment in the framework.

3) *Generalization on DINOv2 Variations:* For generalization, we inspect the self-similarity map (Eq. 1) produced by DINOv2-Small and DINOv2-Large, and select the 2nd and 4th layer respectively for distillation. The mask decoder is then

trained on the distilled image features for few-shot semantic segmentation. Tab. VIII confirms that stronger backbones yield steadily higher mIoU, with the largest gain occurring when switching from DINOv2-Small to DINOv2-Base. Upgrading to DINOv2-Large still helps, but the improvement is modest; This could be attributed to the fact that SAM-H has already transferred most of its knowledge to DINOv2-Base through the bottleneck adapter, leaving limited extra information for the larger model to absorb. Nevertheless, the 60.7% mIoU still exceeds the 58.7% achieved by GF-SAM, that is built on both DINOv2-Large and SAM-H, attesting to the added value of our design. The pretrained models in Tab. VIII can also serve as new foundation models for few-shot semantic segmentation.

VI. CONCLUSION

In summary, we introduce a novel unified framework for few-shot semantic segmentation and its compact variations built upon DINOv2 families. Specifically, in this work, we utilize vision foundation models for few-shot segmentation, finding that DINOv2 features offer strong discriminability across classes. This enables the generation of accurate prior information to guide the segmentation process. To enhance efficiency and accelerate inference, we design a lightweight bottleneck adapter on the third-layer features of DINOv2’s image encoder, which learns from SAM’s encoder through coarse-to-fine distillation. Additionally, we propose a meta-visual prompt generator that leverages the capabilities of large-scale pre-trained models and uses the mask decoder initialized from SAM for complete decoding. For visual prompting, both the semantic-aware visual prompts and Mamba-based dense prompting contributes to the final improvements. Extensive experiments demonstrate the effectiveness of our model, and future work will explore further improvements in accuracy and generalization.

REFERENCES

- [1] Y. Liu, M. Zhu, H. Li, H. Chen, X. Wang, and C. Shen, “Matcher: Segment anything with one shot using all-purpose feature matching,” in *ICLR*, 2024.
- [2] A. Zhang, G. Gao, J. Jiao, C. Liu, and Y. Wei, “Bridge the points: Graph-based few-shot segment anything semantically,” *Advances in Neural Information Processing Systems*, vol. 37, pp. 33 232–33 261, 2025.
- [3] Y. Sun, J. Chen, S. Zhang, X. Zhang, Q. Chen, G. Zhang, E. Ding, J. Wang, and Z. Li, “Vrp-sam: Sam with visual reference prompt,” in *Proceedings of the IEEE/CVF Conference on Computer Vision and Pattern Recognition*, 2024, pp. 23 565–23 574.
- [4] J. Snell, K. Swersky, and R. Zemel, “Prototypical networks for few-shot learning,” *Advances in neural information processing systems*, vol. 30, 2017.
- [5] A. Shaban, S. Bansal, Z. Liu, I. Essa, and B. Boots, “One-shot learning for semantic segmentation,” *arXiv preprint arXiv:1709.03410*, 2017.
- [6] K. Wang, J. H. Liew, Y. Zou, D. Zhou, and J. Feng, “Panet: Few-shot image semantic segmentation with prototype alignment,” in *proceedings of the IEEE/CVF international conference on computer vision*, 2019, pp. 9197–9206.
- [7] Y. Liu, X. Zhang, S. Zhang, and X. He, “Part-aware prototype network for few-shot semantic segmentation,” in *Computer Vision—ECCV 2020: 16th European Conference, Glasgow, UK, August 23–28, 2020, Proceedings, Part IX 16*. Springer, 2020, pp. 142–158.
- [8] B. Yang, C. Liu, B. Li, J. Jiao, and Q. Ye, “Prototype mixture models for few-shot semantic segmentation,” in *Computer Vision—ECCV 2020: 16th European Conference, Glasgow, UK, August 23–28, 2020, Proceedings, Part VIII 16*. Springer, 2020, pp. 763–778.
- [9] B. Zhang, J. Xiao, and T. Qin, “Self-guided and cross-guided learning for few-shot segmentation,” in *Proceedings of the IEEE/CVF conference on computer vision and pattern recognition*, 2021, pp. 8312–8321.
- [10] X. Zhang, Y. Wei, Y. Yang, and T. S. Huang, “Sg-one: Similarity guidance network for one-shot semantic segmentation,” *IEEE transactions on cybernetics*, vol. 50, no. 9, pp. 3855–3865, 2020.
- [11] G. Gao, Z. Fang, C. Han, Y. Wei, C. H. Liu, and S. Yan, “Drnet: Double recalibration network for few-shot semantic segmentation,” *IEEE Transactions on Image Processing*, vol. 31, pp. 6733–6746, 2022.
- [12] Y. Chen, R. Jiang, Y. Zheng, B. Sheng, Z.-X. Yang, and E. Wu, “Dual branch multi-level semantic learning for few-shot segmentation,” *IEEE Transactions on Image Processing*, vol. 33, pp. 1432–1447, 2024.
- [13] G. Zhang, G. Kang, Y. Yang, and Y. Wei, “Few-shot segmentation via cycle-consistent transformer,” *Advances in Neural Information Processing Systems*, vol. 34, pp. 21 984–21 996, 2021.
- [14] E. Iqbal, S. Safarov, and S. Bang, “Msanet: Multi-similarity and attention guidance for boosting few-shot segmentation,” *arXiv preprint arXiv:2206.09667*, 2022.
- [15] B. Peng, Z. Tian, X. Wu, C. Wang, S. Liu, J. Su, and J. Jia, “Hierarchical dense correlation distillation for few-shot segmentation,” in *Proceedings of the IEEE/CVF Conference on Computer Vision and Pattern Recognition*, 2023, pp. 23 641–23 651.
- [16] J. Min, D. Kang, and M. Cho, “Hypercorrelation squeeze for few-shot segmentation,” in *Proceedings of the IEEE/CVF international conference on computer vision*, 2021, pp. 6941–6952.
- [17] S. Hong, S. Cho, J. Nam, S. Lin, and S. Kim, “Cost aggregation with 4d convolutional swin transformer for few-shot segmentation,” in *European Conference on Computer Vision*. Springer, 2022, pp. 108–126.
- [18] Q. Xu, W. Zhao, G. Lin, and C. Long, “Self-calibrated cross attention network for few-shot segmentation,” in *Proceedings of the IEEE/CVF international conference on computer vision*, 2023, pp. 655–665.
- [19] M. Caron, H. Touvron, I. Misra, H. Jégou, J. Mairal, P. Bojanowski, and A. Joulin, “Emerging properties in self-supervised vision transformers,” in *Proceedings of the IEEE/CVF international conference on computer vision*, 2021, pp. 9650–9660.
- [20] M. Oquab, T. Darcet, T. Moutakanni, H. Vo, M. Szafraniec, V. Khalidov, P. Fernandez, D. Haziza, F. Massa, A. El-Nouby *et al.*, “Dinov2: Learning robust visual features without supervision,” *Transactions on Machine Learning Research Journal*, 2024.
- [21] A. Radford, J. W. Kim, C. Hallacy, A. Ramesh, G. Goh, S. Agarwal, G. Sastry, A. Askell, P. Mishkin, J. Clark *et al.*, “Learning transferable visual models from natural language supervision,” in *International conference on machine learning*. PmlR, 2021, pp. 8748–8763.
- [22] A. Kirillov, E. Mintun, N. Ravi, H. Mao, C. Rolland, L. Gustafson, T. Xiao, S. Whitehead, A. C. Berg, W.-Y. Lo *et al.*, “Segment anything,” in *Proceedings of the IEEE/CVF international conference on computer vision*, 2023, pp. 4015–4026.
- [23] W. He, Y. Zhang, W. Zhuo, L. Shen, J. Yang, S. Deng, and L. Sun, “Apsseg: auto-prompt network for cross-domain few-shot semantic segmentation,” in *Proceedings of the IEEE/CVF Conference on Computer Vision and Pattern Recognition*, 2024, pp. 23 762–23 772.
- [24] R. Zhang, Z. Jiang, Z. Guo, S. Yan, J. Pan, X. Ma, H. Dong, P. Gao, and H. Li, “Personalize segment anything model with one shot,” *arXiv preprint arXiv:2305.03048*, 2023.
- [25] L. Meng, S. Lan, H. Li, J. M. Alvarez, Z. Wu, and Y.-G. Jiang, “Segic: Unleashing the emergent correspondence for in-context segmentation,” in *European Conference on Computer Vision*. Springer, 2024, pp. 203–220.
- [26] K. Nguyen and S. Todorovic, “Feature weighting and boosting for few-shot segmentation,” in *Proceedings of the IEEE/CVF international conference on computer vision*, 2019, pp. 622–631.
- [27] O. Ronneberger, P. Fischer, and T. Brox, “U-net: Convolutional networks for biomedical image segmentation,” in *International Conference on Medical image computing and computer-assisted intervention*. Springer, 2015, pp. 234–241.
- [28] V. Badrinarayanan, A. Kendall, and R. Cipolla, “Segnet: A deep convolutional encoder-decoder architecture for image segmentation,” *IEEE transactions on pattern analysis and machine intelligence*, vol. 39, no. 12, pp. 2481–2495, 2017.
- [29] F. Yu and V. Koltun, “Multi-scale context aggregation by dilated convolutions,” *arXiv preprint arXiv:1511.07122*, 2015.
- [30] L.-C. Chen, G. Papandreou, F. Schroff, and H. Adam, “Rethinking atrous convolution for semantic image segmentation,” *arXiv preprint arXiv:1706.05587*, 2017.
- [31] L.-C. Chen, Y. Zhu, G. Papandreou, F. Schroff, and H. Adam, “Encoder-decoder with atrous separable convolution for semantic image segmen-

- tation,” in *Proceedings of the European conference on computer vision (ECCV)*, 2018, pp. 801–818.
- [32] H. Zhao, J. Shi, X. Qi, X. Wang, and J. Jia, “Pyramid scene parsing network,” in *Proceedings of the IEEE conference on computer vision and pattern recognition*, 2017, pp. 2881–2890.
- [33] K. Sun, Y. Zhao, B. Jiang, T. Cheng, B. Xiao, D. Liu, Y. Mu, X. Wang, W. Liu, and J. Wang, “High-resolution representations for labeling pixels and regions,” *arXiv preprint arXiv:1904.04514*, 2019.
- [34] Z. Qin, J. Liu, X. Zhang, M. Tian, A. Zhou, S. Yi, and H. Li, “Pyramid fusion transformer for semantic segmentation,” *IEEE Transactions on Multimedia*, vol. 26, pp. 9630–9643, 2024.
- [35] J. Fu, J. Liu, H. Tian, Y. Li, Y. Bao, Z. Fang, and H. Lu, “Dual attention network for scene segmentation,” in *Proceedings of the IEEE/CVF conference on computer vision and pattern recognition*, 2019, pp. 3146–3154.
- [36] Z. Huang, X. Wang, L. Huang, C. Huang, Y. Wei, and W. Liu, “Ccnnet: Criss-cross attention for semantic segmentation,” in *Proceedings of the IEEE/CVF international conference on computer vision*, 2019, pp. 603–612.
- [37] B. Cheng, I. Misra, A. G. Schwing, A. Kirillov, and R. Girdhar, “Masked-attention mask transformer for universal image segmentation,” in *Proceedings of the IEEE/CVF conference on computer vision and pattern recognition*, 2022, pp. 1290–1299.
- [38] E. Xie, W. Wang, Z. Yu, A. Anandkumar, J. M. Alvarez, and P. Luo, “Segformer: Simple and efficient design for semantic segmentation with transformers,” *Advances in neural information processing systems*, vol. 34, pp. 12077–12090, 2021.
- [39] Q. Wen and C.-G. Li, “Rethinking decoders for transformer-based semantic segmentation: A compression perspective,” *Advances in Neural Information Processing Systems*, vol. 37, pp. 49 806–49 833, 2024.
- [40] J.-Y. Wang, S.-K. Liu, S.-C. Guo, C.-Y. Jiang, and W.-M. Zheng, “Pcnet: Leveraging prototype complementarity to improve prototype affinity for few-shot segmentation,” *Electronics*, vol. 13, no. 1, p. 142, 2023.
- [41] B. Liu, J. Jiao, and Q. Ye, “Harmonic feature activation for few-shot semantic segmentation,” *IEEE Transactions on Image Processing*, vol. 30, pp. 3142–3153, 2021.
- [42] Y. Zhuge and C. Shen, “Deep reasoning network for few-shot semantic segmentation,” in *Proceedings of the 29th ACM International Conference on Multimedia*, 2021, pp. 5344–5352.
- [43] S. Moon, S. S. Sohn, H. Zhou, S. Yoon, V. Pavlovic, M. H. Khan, and M. Kapadia, “Msi: Maximize support-set information for few-shot segmentation,” in *Proceedings of the IEEE/CVF International Conference on Computer Vision*, 2023, pp. 19 266–19 276.
- [44] Z. Lu, S. He, X. Zhu, L. Zhang, Y.-Z. Song, and T. Xiang, “Simpler is better: Few-shot semantic segmentation with classifier weight transformer,” in *Proceedings of the IEEE/CVF International Conference on Computer Vision*, 2021, pp. 8741–8750.
- [45] X. Shi, D. Wei, Y. Zhang, D. Lu, M. Ning, J. Chen, K. Ma, and Y. Zheng, “Dense cross-query-and-support attention weighted mask aggregation for few-shot segmentation,” in *European Conference on Computer Vision*. Springer, 2022, pp. 151–168.
- [46] Z. Chang, X. Gao, N. Li, H. Zhou, and Y. Lu, “Drnet: Disentanglement and recombination network for few-shot semantic segmentation,” *IEEE Transactions on Circuits and Systems for Video Technology*, vol. 34, no. 7, pp. 5560–5574, 2024.
- [47] X. Luo, Z. Tian, T. Zhang, B. Yu, Y. Y. Tang, and J. Jia, “Pfenet++: Boosting few-shot semantic segmentation with the noise-filtered context-aware prior mask,” *IEEE Transactions on Pattern Analysis and Machine Intelligence*, vol. 46, no. 2, pp. 1273–1289, 2023.
- [48] A. Dosovitskiy, L. Beyer, A. Kolesnikov, D. Weissenborn, X. Zhai, T. Unterthiner, M. Dehghani, M. Minderer, G. Heigold, S. Gelly *et al.*, “An image is worth 16x16 words: Transformers for image recognition at scale,” *arXiv preprint arXiv:2010.11929*, 2020.
- [49] S. Chen, F. Meng, R. Zhang, H. Qiu, H. Li, Q. Wu, and L. Xu, “Visual and textual prior guided mask assemble for few-shot segmentation and beyond,” *IEEE Transactions on Multimedia*, vol. 26, pp. 7197–7209, 2024.
- [50] J. Wang, B. Zhang, J. Pang, H. Chen, and W. Liu, “Rethinking prior information generation with clip for few-shot segmentation,” in *Proceedings of the IEEE/CVF Conference on Computer Vision and Pattern Recognition*, 2024, pp. 3941–3951.
- [51] Y. Liu, Y. Tian, Y. Zhao, H. Yu, L. Xie, Y. Wang, Q. Ye, J. Jiao, and Y. Liu, “Vmamba: Visual state space model,” *Advances in neural information processing systems*, vol. 37, pp. 103 031–103 063, 2024.
- [52] M. Everingham, L. Van Gool, C. K. Williams, J. Winn, and A. Zisserman, “The pascal visual object classes (voc) challenge,” *International journal of computer vision*, vol. 88, pp. 303–338, 2010.
- [53] B. Hariharan, P. Arbeláez, L. Bourdev, S. Maji, and J. Malik, “Semantic contours from inverse detectors,” in *2011 international conference on computer vision*. IEEE, 2011, pp. 991–998.
- [54] T.-Y. Lin, M. Maire, S. Belongie, J. Hays, P. Perona, D. Ramanan, P. Dollár, and C. L. Zitnick, “Microsoft coco: Common objects in context,” in *Computer vision—ECCV 2014: 13th European conference, zurich, Switzerland, September 6–12, 2014, proceedings, part v 13*. Springer, 2014, pp. 740–755.
- [55] X. Li, T. Wei, Y. P. Chen, Y.-W. Tai, and C.-K. Tang, “Fss-1000: A 1000-class dataset for few-shot segmentation,” in *Proceedings of the IEEE/CVF conference on computer vision and pattern recognition*, 2020, pp. 2869–2878.
- [56] C. Lang, G. Cheng, B. Tu, and J. Han, “Learning what not to segment: A new perspective on few-shot segmentation,” in *Proceedings of the IEEE/CVF conference on computer vision and pattern recognition*, 2022, pp. 8057–8067.
- [57] Q. Xu, G. Lin, C. C. Loy, C. Long, Z. Li, and R. Zhao, “Eliminating feature ambiguity for few-shot segmentation,” in *European Conference on Computer Vision*. Springer, 2024, pp. 416–433.
- [58] C. Wen, Y. Zhang, J. Fan, H. Zhu, X.-S. Wei, Y. Wang, Z. Kou, and S. Sun, “Object-level correlation for few-shot segmentation,” in *Proceedings of the IEEE/CVF International Conference on Computer Vision*, 2025, pp. 23 689–23 699.
- [59] L. Zhu, T. Chen, J. Yin, S. See, and J. Liu, “Addressing background context bias in few-shot segmentation through iterative modulation,” in *Proceedings of the IEEE/CVF conference on computer vision and pattern recognition*, 2024, pp. 3370–3379.
- [60] S. Park, S. Lee, H. S. Seong, J. Yoo, and J.-P. Heo, “Foreground-covering prototype generation and matching for sam-aided few-shot segmentation,” in *Proceedings of the AAAI Conference on Artificial Intelligence*, vol. 39, no. 6, 2025, pp. 6425–6433.
- [61] X. Wang, W. Wang, Y. Cao, C. Shen, and T. Huang, “Images speak in images: A generalist painter for in-context visual learning,” in *Proceedings of the IEEE/CVF Conference on Computer Vision and Pattern Recognition*, 2023, pp. 6830–6839.
- [62] X. Wang, X. Zhang, Y. Cao, W. Wang, C. Shen, and T. Huang, “Seggpt: Towards segmenting everything in context,” in *Proceedings of the IEEE/CVF International Conference on Computer Vision*, 2023, pp. 1130–1140.